NAWI Graz
Natural Sciences

UNIVERSITY OF GRAZ
Department of Physics

Bachelor's thesis

Geodesics and discrete manifolds within causal dynamical triangulations

Alexander Engertsberger

12214852

in partial fulfilment of the requirements for the degree of
Bachelor - BSc

supervised by Univ.-Prof. Dipl.-Phys. Dr.rer.nat. Axel Torsten Maas

12th July 2025

Abstract

This thesis is a continuation of the work of the bachelor's theses of Lukas Würger [1] and Christina Perner [2], who treated methods of extracting the metric from pre-defined 2-D triangulations in the framework of causal dynamical triangulation (CDT). However, since their work turned out to contain substantial difficulties, the aim of this thesis is to reverse the setup and try to extract possible triangulations from different given metrics. Moreover, geodesic integrals around singularities were investigated, as they are of interest for CDT. After treating the simple case of 2-D Minkowski space, the thesis turns to more advanced geometries: the 2-sphere and the Schwarzschild geometry. For the 2-sphere, promising results were obtained, although the transcendental nature of the geodesic equations posed challenges for finding analytical expressions. Nevertheless, the numerical implementation of these methods demonstrated how the framework can still be applied effectively. For the Schwarzschild geometry, geodesic expressions were successfully constructed in the radial case, while computational challenges prevented a systematic search for true equilateral simplices.

Contents

1 Introduction

General relativity (GR) and the standard model are the two pillars of modern theoretical physics. In a nutshell, the standard model is a theory explaining all fundamental forces except gravity, and their interaction with matter (fermions). Each fundamental force has its own carrier (gauge bosons):

- Weak force: W and Z bosons
- Strong force: Gluons g
- Electromagnetic force: Photons γ

The standard model is one case of a more general family of physical theories: It is a *field theory*. For each boson (in fact for every particle in the standard model), there exists a corresponding field (similar to the vector potential in electrodynamics). In GR however, the field describing the gravitational force is spacetime *itself*! As a consequence, one often hears that gravity isn't regarded as a force at all, but rather as a manifestation of the curvature of space and time. The hypothetical particle corresponding to this field is the *graviton*, which has not been detected yet.

While both theories work wonderfully in their respective domain, GR breaks down at scales near the Planck length (1.62×10^{-33} cm), the Planck time (5.39×10^{-44} s) and the Planck energy (1.22×10^{19} GeV), as quantum fluctuations begin to play a significant role [3]. As countless tests have confirmed both theories on their domain, and they are yet to be falsified by an experiment, several attempts have been made at finding an underlying theory that contains both the standard model and GR in the limit of high energies and large scales. One famous example of such a 'theory of everything' is *string theory*. While theorists have been working on string theory for over 50 years now, there has not yet been a single experiment confirming that it is indeed the reality we live in. As a consequence, many other theories try to deliver a quantized description of gravity.

One example is *causal dynamical triangulation* (CDT), which is the framework from which this thesis arose. However, it focuses solely on quantizing gravity while not trying to describe other interactions. It is therefore *not* a theory of everything. The present thesis will first give an overview of the theoretical basics designed to prepare a physics student at the end of their bachelor's degree for the subsequent chapters. In the main part, we will first address the simple case of flat Minkowski spacetime, before moving on to the intrinsic geometry of the 2-D sphere (2-sphere), including introductory numerical calculations. The thesis then closes with an introduction to the 4-D Schwarzschild geometry, including methods for extracting a triangulation.

2 Theoretical background

Throughout this thesis, vectors will be written in bold, while scalars and vector components will be displayed as usual in italics.[1] In this notation, we will not differentiate between abstract vectors and lists of components (coordinate vectors).

2.1 Linear algebra

I assume that the reader is familiar with the key concepts of linear algebra. However, since GR and differential geometry are built upon rather abstract formulations, I want to give a brief overview of important concepts and notations.

The idea of vectors commonly used when first studying linear algebra (as a physicist) is that a three-dimensional physical quantity characterized by a magnitude and direction can be specified

[1] This is different from the notation used for example by Hartle [3]. He uses boldface notation only for four-vectors and an arrow ($\vec{v}$) for three-vectors. However, this notation runs into problems when dealing with dimensions different from 3 and 4.

by measuring this magnitude (e.g. its length) along a basis of three different directions $\mathbf{e}_1, \mathbf{e}_2, \mathbf{e}_3$. If we label these *components* with a, b, c we can represent it by these numbers

$$\mathbf{v} \mathrel{\widehat{=}} \begin{pmatrix} a \\ b \\ c \end{pmatrix}. \tag{2.1}$$

However, this is just a shorthand notation for the basis representation of this vector which can be written more clearly as

$$\mathbf{v} = a\mathbf{e}_1 + b\mathbf{e}_2 + c\mathbf{e}_3, \tag{2.2}$$

where $(\mathbf{e}_i)$ is an arbitrary Cartesian basis. However, if one chose any other basis of our vector space and the components in (2.1) would look different, even though they represent the same vector (the $\mathrel{\widehat{=}}$ symbol indicates 'is represented by').

When dealing with vector spaces of arbitrary dimensions, it is wiser to simplify the notation used in Eq. (2.2) by using a summation symbol $\sum$. However, it is much easier to omit this symbol altogether and to use the *Einstein summation convention*, where one sums over the whole range of identical indices when they occur pairwise in the sub- and superscript. If we label a, b, c from the equation above with superscript indices v^1, v^2, v^3 we can write it as follows[2]:

$$\mathbf{v} = v^i \mathbf{e}_i \ .$$

Note that the indices must not necessarily belong to two different entities when using the summation convention, e.g. the trace of a linear map $F : V \to V$ can be written as

$$\mathrm{Tr}(F) \equiv F^k{}_k \ .$$

The question then arises how exactly vector components transform during a change of basis. It is helpful to introduce the following:

Definition 2.1. Let V be a vector space over a field $\mathbb{K}$ with two different bases $(\mathbf{e}_k)_{k=1,\dots,n}$ and $(\mathbf{e}_{k'})_{k'=1,\dots,n}$. The linear map $S : V \to V$ is called a *transition matrix* if

$$\mathbf{e}_{l'} = S^k{}_{l'}\, \mathbf{e}_k \ . \tag{2.3}$$

We know that every basis change can be regarded as such a matrix S, because Eq. (2.3) implies that the columns of S must be the components of the new basis vectors represented in our old basis. One can then prove that the transition matrix is regular, and its inverse corresponds to the transition matrix in the opposite direction. Note that the primed indices indicate different vectors, e.g. $\mathbf{e}_{1'} \neq \mathbf{e}_1$.

It is easy to see how our vector components change correspondingly. Using the two bases from Def. 2.1, we have:

$$\mathbf{v} = v^k \mathbf{e}_k = v^{k'} \mathbf{e}_{k'} = v^{k'} S^i{}_{k'}\, \mathbf{e}_i .$$

This of course implies that $v^i = S^i{}_{k'}\, v^{k'}$. The fact that the vector components transform oppositely as the basis vectors is the reason why they are sometimes also referred to as *contravariant* vectors [4]. Alternatively we could also write this as $v^k = S^k{}_{k'}\, v^{k'}$, since the primed indices indicate a change of basis.[3]

Analogously to vectors, we can define multidimensional lists of numbers, which transform similarly during a change of basis: Tensors. If we label the components of the inverse of S with $T^{k'}{}_l$, which implies that $S^m{}_{k'}\, T^{k'}{}_n = \delta^m_n$. A tensor X of type (r, s) then transforms as follows:

$$X^{k'_1 \cdots k'_r}{}_{l'_1 \cdots l'_s} = S^{k'_1}{}_{k_1} \cdots S^{k'_r}{}_{k_r}\, T^{l_1}{}_{l'_1} \cdots T^{l_s}{}_{l'_s}\, X^{k_1 \cdots k_r}{}_{l_1 \cdots l_s} \ .$$

In fact, tensors are *defined* by objects which transform in this way. A vector is therefore a type $(1, 0)$ tensor.

[2] Not to be mistaken with powers of v.

[3] This is the convention Carroll uses in his GR book [5].

2.2 Differential geometry and topology

We will now define some important terminology. The precise definitions will make understanding the concepts in later chapters easier, and explain why multiple coordinate systems are sometimes needed. Even though we will get rid of some of the pedantic precision when actually working with the concepts, it is still useful to review the exact definitions.

Definition 2.2. Let X, Y be two topological spaces. A function $f : X \to W$ is a *homeomorphism*, if f^{-1} exists and both f and f^{-1} are continuous. If such a function exists, X and Y are considered *homeomorphic* [6].

For the sake of the argument let us look at

$$\mathbf{r} : \begin{cases} U \to M \\ (x^1, \dots, x^n) \mapsto \mathbf{r}(x^1, \dots, x^n) \end{cases} \quad , \quad U \subset \mathbb{R}^n,\ M \subset \mathbb{R}^N \ ,$$

with $n \leq N$. We can also regard $\mathbf{r}$ as N maps from U to $\mathbb{R}$. $\mathbf{r}$ is then called *regular* iff it is smooth and the Jacobian matrix $\left(\frac{\partial r_i}{\partial x_j}\right)$ has a maximal rank (rank n) at every $\mathbf{x}_0 \in U$. This leads us to the following definition:

Definition 2.3. Let $M \subset \mathbb{R}^N$ be our manifold. Further let $U \subset \mathbb{R}^n$ be an open set and $\mathbf{r} : U \to M$ be an injective map. The pair $(\mathbf{r}, U)$ is then called a *coordinate system* if [7]:

i) $\mathbf{r}$ is a homeomorphism and the set $\mathbf{r}(U)$ is also open.

ii) $\mathbf{r}$ is smooth and regular.

Note: The first point in the definition above makes $\mathbf{r}$ 'respect' the topology of M.

Similar to the transition matrix of Cartesian coordinate systems in Def. 2.1, we can introduce transition functions for arbitrary (often curvilinear) coordinate systems. Suppose we have two coordinate systems $(\mathbf{r}_1, U_1)$ and $(\mathbf{r}_2, U_2)$. The functions $\mathbf{r}_1$, $\mathbf{r}_2$ will cover different areas of the manifold M. Suppose there exist an overlap region $\mathbf{r}_1(U_1) \cap \mathbf{r}_2(U_2)$ on M, then we can define the following *transition functions*:

$$\mathbf{r}_{21} : \begin{cases} U_{12} \to U_{21} \\ \mathbf{x} \mapsto (\mathbf{r}_2^{-1} \circ \mathbf{r}_1)(\mathbf{x}) \end{cases} \quad , \qquad \mathbf{r}_{12} : \begin{cases} U_{21} \to U_{12} \\ \mathbf{x} \mapsto (\mathbf{r}_1^{-1} \circ \mathbf{r}_2)(\mathbf{x}) \end{cases} \quad , \tag{2.4a}$$

$$\text{where} \qquad U_{12} = \mathbf{r}_1^{-1}(\mathbf{r}_1(U_1) \cap \mathbf{r}_2(U_2)), \tag{2.4b}$$

$$U_{21} = \mathbf{r}_2^{-1}(\mathbf{r}_1(U_1) \cap \mathbf{r}_2(U_2)) \ . \tag{2.4c}$$

These functions can of course only be defined on the respective preimage of the overlap region. They then work essentially the same as the transition matrix, i.e. we can plug in the coordinates in one coordinate system and the function gives us the coordinates of the same vector described by the other coordinate system. We can now introduce the important concept of an atlas:

Definition 2.4. A family of coordinate systems $(\mathbf{r}_i, U_i)_i$ on M is called an *atlas*, if it covers M, so $M \subset \bigcup_i \mathbf{r}_i(U_i)$, and between each pair of coordinate systems exist smooth transition functions [7].

2.3 Theory of relativity

We will now turn to metrics. They are technically still a part of differential geometry but since they are such an integral part of GR and this thesis, they will serve as an excellent introduction to relativity.

Definition 2.5. [7] The *metric* g is a (0,2) tensor on M, which defines the scalar product:

$$g(\mathbf{u}, \mathbf{v}) := g_{\mu\nu} u^\mu v^\nu,$$

and is symmetric in its components, $g_{\mu\nu} = g_{\nu\mu}$, and also satisfies $g(\mathbf{u}, \mathbf{u}) \geq 0$. [4]

The metric thus raises or lowers vector components in the following way:

$$g_{ij} v^j = v_i.$$

Furthermore, the positive definiteness and symmetry of g fulfil the axioms of a metric in the common sense, and therefore gives us a notion of 'distance'.
At this point it must be mentioned that v^i and v_i generally do not have the same components. However, in Euclidean space, where $g_{ij} = \delta_{ij}$, the components of vectors and covectors are equal, which is why we do not differentiate between them normally.

2.3.1 Special relativity

The topology of our universe, *spacetime*, is a four-dimensional manifold. We further demand from the topology that locally (if we 'zoom in' far enough), it looks like 'flat' Minkowski space. Minkowski space is the spacetime in the absence of gravity ('flat' spacetime), which arises from the fact that the speed of light, c, is constant in every inertial frame (see [3] for an intuitive introduction to relativity).

This thesis will use the notation that indices denoted with Greek letters ($\alpha, \beta, \ldots$) will run from 0 to 3, while Latin indices ($i, j, \ldots$) will run from 1 to 3. In Minkowski spacetime, the index 0 corresponds to the time multiplied by the speed of light, ct, and 1 through 3 correspond to x, y and z. Furthermore, we will use geometrized units, in which we set the speed of light and the gravitational constant to one, i.e. $c = G = 1$. Therefore, length, time and mass will all have the same units (meters). The geometry of flat spacetime is given by the Minkowski metric $\eta_{\mu\nu}$. The sign of the Minkowski metric is dependent on convention, we will use the signature $(-,+,+,+)$:

$$(\eta_{\mu\nu}) = \mathrm{diag}(-1, 1, 1, 1) = \begin{pmatrix} -1 & 0 & 0 & 0 \\ 0 & 1 & 0 & 0 \\ 0 & 0 & 1 & 0 \\ 0 & 0 & 0 & 1 \end{pmatrix}. \tag{2.5}$$

The key characteristic of flat spacetime is that the discrete spacetime interval

$$\Delta s^2 = \eta_{\mu\nu} \Delta x^\mu \Delta x^\nu \tag{2.6}$$

between two events stays invariant under a change of basis. This means that the components of the metric in (2.5) must stay the same in every coordinate system. In fact, the basis transformations Λ, which are called *Lorentz transformations* in flat spacetime, are *defined* by this constraint:

$$\eta_{\mu'\nu'} = \Lambda^{\mu}{}_{\mu'} \Lambda^{\mu'}{}_{\mu} \eta_{\mu\nu}.$$

Traditionally, 2-D spacetime diagrams are arranged so that the x^1 coordinate is the horizontal axis and the x^0 the vertical one (Fig 2.1). From Eq. (2.5) and (2.6) it becomes obvious, that (Δs) between two events in spacetime can be smaller, greater, or equal to zero. We give these cases the names as seen in Fig. 2.1. Thus, spacelike-separated events are not causally connected, i.e. there is no particle path (not even light) which could pass through both events.

[4] Technically, the scalar product is defined on the tangent vector space T_p, but we will disregard this for our discussion.

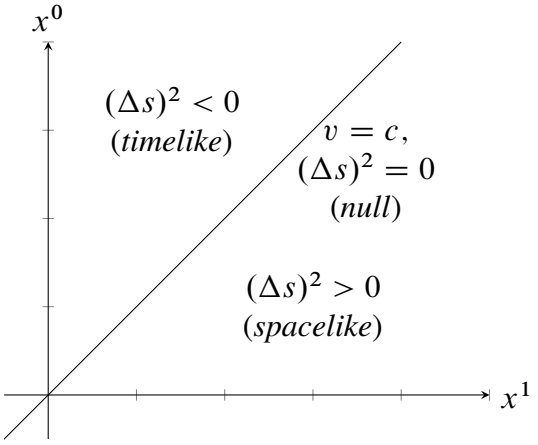

Figure 2.1: Representation of differently separated events with reference to the origin in the Minkowski diagram.

Δs^2 gives the spacetime a measure of distance between two events. Therefore, to get the length of a parameterized curve with coordinates (x^μ). The infinitesimal spacetime distance is simply:

$$ds^2 = \eta_{\mu\nu} dx^\mu dx^\nu. \tag{2.7}$$

If we wanted to integrate over ds we would have to distinguish between timelike and spacelike curves. Luckily, these two do not mix: All particles move along timelike curves; photons move along null curves; and tachyons would move along spacelike curves [3, 5]. Even though tachyons are only hypothetical, nothing can stop us from still looking at spacelike connections and calculating their length - in fact, this is exactly what I am going to do later. We therefore have two different integrals we can evaluate:

$$\begin{aligned} \text{for spacelike curves:} \quad \Delta s &= \int \sqrt{\eta_{\mu\nu} \frac{dx^\mu}{d\lambda} \frac{dx^\nu}{d\lambda}}\, d\lambda, \\ \text{for timelike curves:} \quad \Delta \tau &= \int \sqrt{-\eta_{\mu\nu} \frac{dx^\mu}{d\lambda} \frac{dx^\nu}{d\lambda}}\, d\lambda. \end{aligned} \tag{2.8}$$

In fact $\Delta\tau$, the proper time (German: *Eigenzeit*), is the time an observer would measure when moving along the trajectory. These integrals give the spacetime a meaning of 'straight' paths: A straight trajectory is defined by the path that *maximizes* the proper time. In flat space, this becomes quite obvious: A pair of twins, Alice and Bob, are both located at the same time and place on earth (neglecting both the rotation and gravity of earth). While Alice remains on earth, Bob hops on a spaceship and starts moving away from earth with a speed close to c. Quite famously, after his return to earth Bob has aged less than Alice. The simple reason for this asymmetry is that while Alice was moving along a straight path through spacetime, Bob was not, as he had to turn around back to earth halfway through his journey, which lead to a shorter proper time for Bob. This example should illustrate that straight paths between two events have the longest proper time of all paths.

We can interpret the integrands of (2.8) as an action, with a Lagrangian $\mathcal{L}$ for timelike curves:

$$\mathcal{L} = \sqrt{-\eta_{\mu\nu} \frac{dx^\mu}{d\lambda} \frac{dx^\nu}{d\lambda}}.$$

The differential equations can then be calculated through the Euler-Lagrange equations

$$\frac{d}{dt} \frac{\partial \mathcal{L}}{\partial \dot{x}^\mu} - \frac{\partial \mathcal{L}}{\partial x^\mu} = 0,$$

where $\dot{x}^\mu$ is a shorthand notation for $\frac{dx^\mu}{d\lambda}$.

Very often however, it is easier to use the altered Lagrangian

$$F := \frac{1}{2}\mathcal{L}^2 = \frac{1}{2}\left(-\eta_{\mu\nu}\frac{dx^\mu}{d\tau}\frac{dx^\nu}{d\tau}\right) \tag{2.9}$$

instead, where we parameterize our curve with the proper time τ instead of an arbitrary λ, which simplifies the Euler-Lagrange equations slightly. It is then quite easy to show that it is indeed true:

$$\frac{d}{d\tau}\frac{\partial F}{\partial \dot{x}^\mu} - \frac{\partial F}{\partial x^\mu} = \frac{d\mathcal{L}}{d\tau}\frac{\partial \mathcal{L}}{\partial \dot{x}^\mu} + \mathcal{L}\left(\frac{d}{d\tau}\frac{\partial \mathcal{L}}{\partial \dot{x}^\mu} - \frac{\partial \mathcal{L}}{\partial x^\mu}\right) = \frac{d\mathcal{L}}{d\tau}\frac{\partial \mathcal{L}}{\partial \dot{x}^\mu} = 0,$$

where in the last step one can exploit that $\mathcal{L} = -\eta_{\mu\nu}\frac{dx^\mu}{d\tau}\frac{dx^\nu}{d\tau} = 1$ is just the negative norm of the four-velocity [5]. The same follows for spacelike curves, where we parameterize with s instead. Furthermore, this is also true for arbitrary metrics g, where we will turn to now.

2.3.2 General relativity

In special relativity (flat spacetime), straight line paths between two timelike separated events *maximize* the proper time in (2.8). The situation is similar in GR in that sense that straight line paths still *extremize* the action but not necessarily maximize it [3]. The Minkowski metric in the line element of Eq. (2.7) is replaced by an arbitrary metric $g_{\mu\nu}$:

$$ds^2 = g_{\mu\nu}dx^\mu dx^\nu.$$

While $g_{\mu\nu}$ will still be a symmetric matrix, its components are generally functions of the coordinates and therefore not constant in space and time. Two metrics describing the same geometry can have different components when using different coordinate systems [3]. Similar to the transition matrices, the inverse metric $g^{\mu\nu}$ is defined by [5]

$$g^{\mu\nu}g_{\nu\rho} = \delta^\mu_\rho\ . \tag{2.10}$$

The differential equations arising from minimizing the action can be written in a general form as [5]:

$$\frac{d^2x^\mu}{d\lambda^2} + \Gamma^\mu_{\rho\sigma}\frac{dx^\rho}{d\lambda}\frac{dx^\sigma}{d\lambda} = 0, \tag{2.11}$$

which are called the *geodesic equations* for $\mu = 0, \ldots, 1$. The coefficients $\Gamma^\mu_{\rho\sigma}$ are called *Christoffel symbols* and can be calculated by [5]:

$$\Gamma^\mu_{\rho\sigma} = \frac{1}{2}g^{\mu\nu}(\partial_\rho g_{\sigma\nu} + \partial_\sigma g_{\nu\rho} - \partial_\nu g_{\rho\sigma}), \tag{2.12}$$

where $\partial_\alpha \equiv \partial/\partial x^\alpha$. Furthermore, they are symmetric in the lower indices: $\Gamma^\mu_{\rho\sigma} = \Gamma^\mu_{\sigma\rho}$. However, for our purpose it is often easier to extract the geodesic equation not by calculating the Christoffel symbols, but by calculating the Euler-Lagrange equations resulting from extremizing the action.

The Einstein field equations tell us how the curvature of spacetime reacts to mass and energy distributions:

$$R_{\mu\nu} - \tfrac{1}{2}Rg_{\mu\nu} = 8\pi G T_{\mu\nu}\ ,$$

where $R_{\mu\nu}$ is the Ricci curvature tensor, R the scalar curvature, $g_{\mu\nu}$ is the metric, $T_{\mu\nu}$ is the stress-energy tensor and G is the gravitational constant. Historically, Karl Schwarzschild provided the first exact solution to Einstein's equation in 1916, for a spherical source of curvature (like a star or a black hole). We will however not concern with Einstein's equation at all but rather just use the Schwarzschild metric as it is, to investigate its geometry.

2.4 Causal dynamical triangulation

Causal dynamical triangulation (CDT) is a non-perturbative theory of quantum gravity, which means that it does not add any extra structure to the physical system of GR (unlike the extra dimensions of string theory). It is based on Regge calculus, which is a discretized version of GR, consisting of four-dimensional simplices of spacetime [8]. Similar to the discretization of the dome in Fig. 2.2, the simplices in itself are flat - only in the way of their arrangement does the curvature arise [9]. Without getting into too much detail, the reason for doing this is that it allows to get from the gravitational path integral formulation

$$Z = \int \mathcal{D}[g]\, e^{iS[g]},$$

where g is the metric and we sum over all virtual paths, to a discrete version of it:

$$Z = \lim_{N_4 \to \infty} \sum_{\text{causal } T} \frac{1}{C(T)}\, e^{iS[T]},$$

where we replaced the Einstein-Hilbert action $S[g]$ with the simplicial version of it, $C(T)$ is the number of symmetries of the possible triangulations (to account for equivalent triangulations) and N_4 is the amount of simplices included (the limit refers to the continuous case) [9, 10].

In 2-D, the simplices (triangles) have two timelike edges with length $\Delta\tau = a$ and one spacelike edge with length $\Delta s = a$ [8]. In this thesis, we will set $a = 1$ for simplicity.

Figure 2.2: Discretization of the surface of a radio telescope in Itapetinga, Brazil [11].

3 Triangulation of the 2-D Minkowski spacetime

The first goal of this thesis is to create a triangulation in a two-dimensional Minkowski space. Since we only have one time and one spacial dimension, one may set $x^2 = x^3 = 0$, and as usual $x^0 = t$ and $x^1 = x$.

With the Minkowski metric (2.5), our altered Lagrangian for timelike geodesics from Eq. (2.9) now becomes:

$$F = \frac{1}{2}\left[\left(\frac{dt}{d\tau}\right)^2 - \left(\frac{dx}{d\tau}\right)^2\right]. \tag{3.1}$$

It is then easy to see that the Euler-Lagrange equations are

$$\frac{d^2t}{d\tau^2} = 0, \quad \frac{d^2x}{d\tau^2} = 0,$$

which we can solve as follows:

$$\begin{aligned} \frac{d}{d\tau}\frac{dt}{d\tau} = \frac{d}{d\tau}\gamma = 0 \implies v = \text{const.}, \quad t(\tau) = \gamma\tau + t_0, \\ \frac{d^2x}{d\tau^2} = 0 \implies x(\tau) = \alpha\tau + x_0, \end{aligned}$$

where t_0, x_0 and α are constants, and we have used the time dilation formula $d\tau = dt/\gamma$. However, because the norm of the four-velocity has to be -1, there is an additional constraint on α:

$$\eta_{\mu\nu}\frac{dx^\mu}{d\tau}\frac{dx^\nu}{d\tau} = -1 \implies -\gamma^2 + \alpha^2 = -1 \implies \alpha = \sqrt{\gamma^2 - 1} = v\gamma. \tag{3.2}$$

We can now however easily switch back to our coordinate time t and write our path as:

$$\mathbf{x}(t) = (\gamma\tau + t_0, v\gamma\tau + x_0) = (t,\ v\,(t - t_0) + x_0), \tag{3.3}$$

which is, trivially, the graph of a straight line. What we have shown therefore is that the discrete spacetime interval in Eq. (2.6) is indeed the geodesic distance between two events.

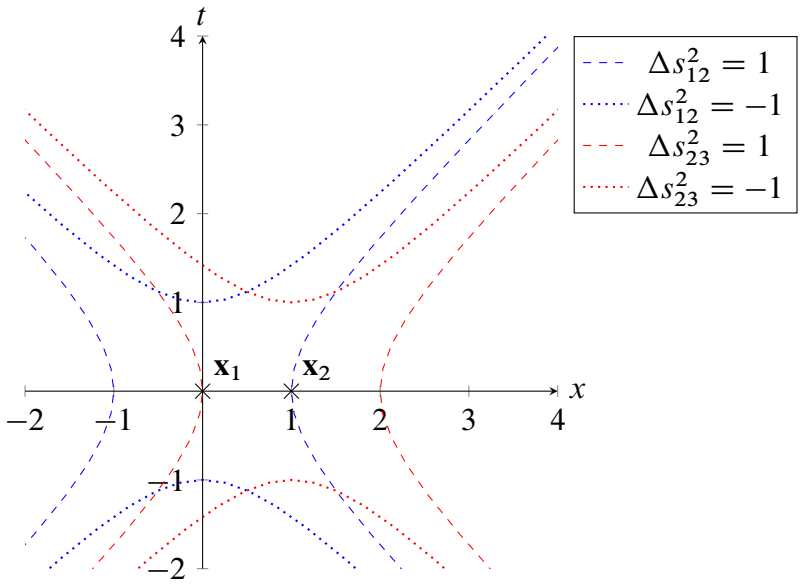

Figure 3.1: Illustration of equidistant points away from $\mathbf{x}_1$ in blue away from $\mathbf{x}_2$ in red. Dotted: timelike. Dashed: spacelike.

To start the triangulation process we are completely free in our choice for the first point and might as well choose the origin $(x_1^\mu) = (0,0)$. To can then calculate, which events are a 'distance' $\Delta s^2 = \pm 1$ away:

$$(\Delta s_{12})^2 = \eta_{\mu\nu}(x_1^\mu - x_2^\mu)(x_1^\nu - x_2^\nu) = -(x_2^0)^2 + (x_2^1)^2 \stackrel{!}{=} \pm 1.$$

This conditions are satisfied by the functions:

$$\begin{aligned}(\Delta s_{12})^2 = +1: &\quad (x_2^\mu(\lambda)) = (\pm\cosh\lambda, \sinh\lambda),\\ (\Delta s_{12})^2 = -1: &\quad (x_2^\mu(\lambda)) = (\sinh\lambda, \pm\cosh\lambda),\end{aligned}$$

which are the generalizations of a circle in the non-Euclidean metric of flat spacetime. The functions are visualized through the blue lines in Fig. 3.1. Since CDT requires one spacelike connection, we can choose the event lying on the x^1-axis as our next event, i.e. $(x_2^\mu) = (0,1)$. The third point must then satisfy a system of two equations, where $(\Delta s_{23})^2 = (\Delta s_{13})^2 = -1$, since the other two connections must be timelike in CDT. The solutions for this system would be the intersections between the dotted red and blue lines in Fig. 3.1. The choice between the top and bottom intersection already indicate the shape of the two triangles needed for filling the whole space:

$$-(x_3^0)^2 + (x_3^1)^2 = -1, \quad -(x_3^0)^2 + (x_3^1 - 1)^2 = -1 \implies (x_3^\mu) = \left(\pm\frac{\sqrt{5}}{2}, \frac{1}{2}\right).$$

The triangulated grid resulting from these choices is visualized in Fig. 3.2a, in which the axis-ratio was set to suggest equilateral triangles. As a remark, there is an infinite amount of triangulations, as the choice of the spacelike point, i.e. $\mathbf{x}_2$, can be chosen anywhere on the blue dashed line in Fig. 3.1. An extremer example of a possible triangulation is provided in Fig. 3.2b. We can go from Fig. 3.2a to 3.2b by a Lorentz transformation, since they leave the spacetime intervals unchanged.

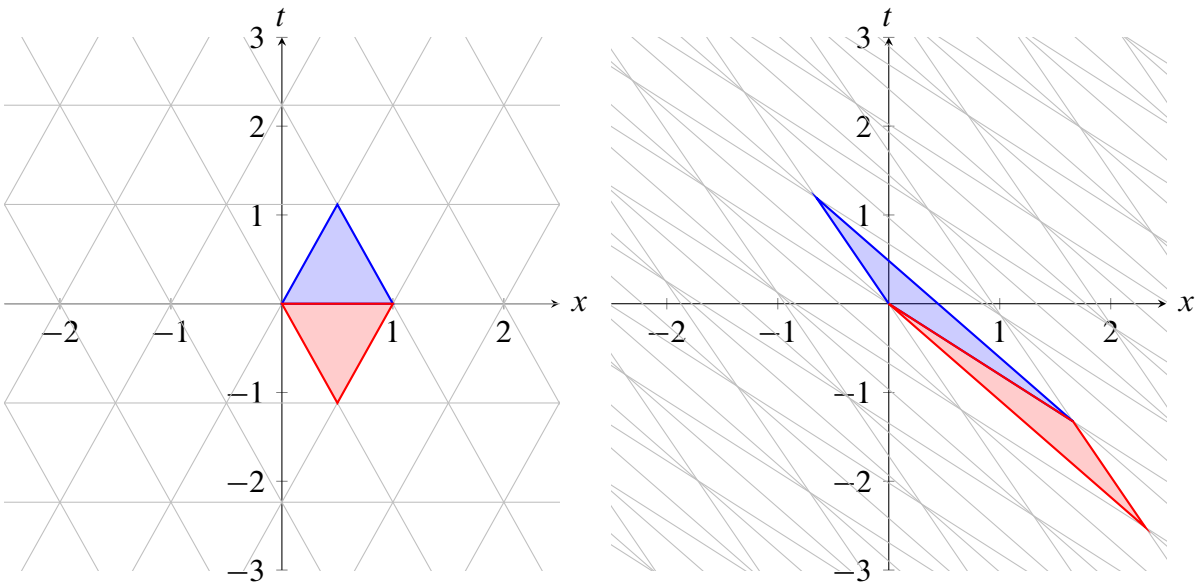

(a) **(b)**

Figure 3.2: Example of possible triangulation for a 2D-Minkowski grid with the two elementary building blocks in blue and red. (**a**) Horizontal lines are $\Delta t = \sqrt{5}/2$ apart. (**b**) Extremer example of valid triangulation.

Furthermore, it must be mentioned that the grid in Fig. 3.2a cannot be physically visualized in a Euclidean geometric sense (by a rigid object). The blue triangle however can perhaps be imagined by a rod of length 1, becoming smaller and smaller until it ceases to exist after a time of $\sqrt{5}/2$ m (since we measure time in meters). Nevertheless, the Minkowski space diagram is still a helpful geometric representation of particle word lines, when considered that longer distances on paper does not equal longer spacetime distances (as shown by Fig. 3.2).

4 Triangulation of the 2-sphere

An example of a curved, two-dimensional manifold is the 2-sphere S^2. It is a subset of $\mathbb{R}^2$ given by [7]:

$$S^2 := \{\mathbf{x} \in \mathbb{R}^3 \mid (x^1)^2 + (x^2)^2 + (x^3)^2 = R^2\}. \tag{4.1}$$

Using the spherical coordinates (θ, ϕ), the metric and line element become [3, 7]:

$$(g_{ij}) = R^2 \begin{pmatrix} 1 & 0 \\ 0 & \sin^2\theta, \end{pmatrix} \iff ds^2 = R^2(d\theta^2 + \sin^2\theta\, d\phi^2). \tag{4.2}$$

However, not every point on S^2 can be represented by a single spherical coordinate system, as including the poles would destroy the injectivity of the coordinate function. One possible way to set up a coordinate system would be:

$$\mathbf{r}(\theta, \phi) = R \begin{pmatrix} \sin\theta\cos\phi \\ \sin\theta\sin\phi \\ \cos\theta \end{pmatrix}, \quad \theta \in (\pi/5, 4\pi/5),\ \phi \in [0, 2\pi), \tag{4.3}$$

where 2 domes at the north and south poles are 'cut out'.

4.1 Single coordinate system

We will turn to our full atlas later, and will now only look at geodesics within the bounds of the coordinate system in (4.3).

4.1.1 Analytical solution

The differential equations resulting from the Lagrangian (2.9) can be solved for example by setting ($\theta = \pi/2$, $d\theta = 0$), which leads to the equation for a great circle (in this case the equator). However, it would be more practical to find an expression for a geodesic between two arbitrary points (θ_1, ϕ_1) and (θ_2, ϕ_2). It turns out to be wiser to instead minimize the action

$$\Delta s = \int \sqrt{g_{ij}dx^i dx^j} = \int \sqrt{d\theta^2 + \sin^2\theta\, d\phi^2} = \int \sqrt{1 + \sin^2\theta \left(\frac{d\phi}{d\theta}\right)^2}\, d\theta, \tag{4.4}$$

where we assumed $d\theta \neq 0$. In the case of $d\theta = 0$ the geodesic just becomes the equator. It is not possible to square the Lagrangian in (4.4), since we did not use a natural parametrization. Using $\phi' := d\phi/d\theta$, the Euler-Lagrange equation becomes:

$$\frac{\sin^2\theta\,\phi'}{\sqrt{1 + \sin^2\theta\,\phi'^2}} = C = \text{const.} \tag{4.5a}$$

$$\implies \phi' = \frac{C}{\sin\theta\sqrt{\sin^2\theta - C^2}}. \tag{4.5b}$$

This can be solved by simple integration and leads to the following expression:

$$\phi(\theta) = \arccos\Big(\tfrac{1}{C_1}\cot\theta\Big) + C_2, \quad \text{or implicitly:} \quad \cot\theta = C_1\cos(\phi_1 - C_2), \tag{4.6}$$

where $C_1 = \sqrt{1/C^2 - 1}$. The full derivation of the integral can be seen in Eq. (A.1) of the appendix. The constants C_1, C_2 are determined by the start point (θ_1, ϕ_1) and end point (θ_2, ϕ_2) of the geodesic, i.e. $\phi(\theta_1) = \phi_1$ and $\phi(\theta_2) = \phi_2$. Since we presumed $d\phi \neq 0$ one constraint of this geodesic is that $\phi_1 \neq \phi_2$. We can then calculate the constants:

$$\left.\begin{aligned}\cot\theta_1 &= C_1\cos(\phi_1 - C_2)\\ \cot\theta_2 &= C_1\cos(\phi_2 - C_2)\end{aligned}\right\} \implies \cos(\phi_2 - \phi_0) = K\cos(\phi_1 - \phi_0), \quad \text{where} \quad K = \frac{\cot\theta_2}{\cot\theta_1}$$

$$\implies C_2 = \arctan\frac{\cos\phi_2 - K\cos\phi_1}{K\sin\phi_1 - \sin\phi_2}, \quad C_1 = \frac{\cot\theta_1}{\cos(\phi_1 - \phi_0)},$$

where we assumed $\theta_1 \neq \pi/2$. Furthermore, the $\arctan(\cdot)$ must in fact be changed to a two-valued function to accommodate for the whole range of ϕ, as we will see later.

It turns out to be possible to find analytical expressions for C_1 and C_2 for certain start and end points, but due to the transcendental nature of the equation, not for arbitrary boundaries. If it were possible to get a general expression for C_1 and C_2, then one could use it to calculate the geodesic length by Eq. (4.4). In fact, this integral is solvable even for arbitrary C_1, C_2 but the solution is so complicated that there is little hope for using it to set up solvable systems of equations with it.

However, once an equilateral triangle is found, the rest of the surface could technically be covered by symmetry transformations (rotations) of copies of this triangle. To find two points which are geodesic distance of 1 apart, one could start with a known geodesic parametrization. Leaving either ϕ constant while varying θ or fixing $\theta = \pi/2$ while varying ϕ will lead to great circles (longitudes and the equator). We can therefore start with the point $\mathbf{x}_1 = (\pi/2, 0)$, which lies on the geodesic $\mathbf{x}(\lambda) = (\lambda, 0)$ where $\lambda \in [0, \pi)$. To find a point a geodesic distance of 1 apart, we can calculate the (trivial) integral resulting from (4.4):

$$\Delta s = \int_{\pi/2}^{\lambda_0} R\,d\lambda = R\Big(\lambda_0 - \frac{\pi}{2}\Big) \overset{!}{=} 1 \implies \lambda_0 = \frac{\pi}{2} + \frac{1}{R}. \tag{4.7}$$

This means that the second vertex can be located at $\mathbf{x}_2 = (\pi/2 + 1/R, 0)$. Finding the third point imposes a greater challenge, as we do not know the geodesic it will lie on in advance (note that latitudinal lines are *not* geodesics).

To calculate the geodesic distance between to arbitrary points, it is easiest to refer to the coordinate system in (4.3) and calculate the central angle α between the two points by the dot product:

$$\mathbf{r}(\theta_1, \phi_1)\cdot\mathbf{r}(\theta_2, \phi_2) = R^2\cos\alpha \tag{4.8a}$$

$$\implies \alpha = \arccos(\sin\theta_1\sin\theta_2\cos(\phi_1 - \phi_2) + \cos\theta_1\cos\theta_2). \tag{4.8b}$$

Even though we could only calculate this by referring to our extrinsic coordinates (x, y, z), the central angle α will be invariant under coordinate changes because it was calculated by a scalar product. Because the curvature of the sphere is the same at every point, it is possible to calculate the geodesic distance $\Delta s \equiv s(\mathbf{x}, \mathbf{y})$ by

$$s((\theta_1, \phi_1), (\theta_2, \phi_2)) = R\alpha = R\arccos(\sin\theta_1\sin\theta_2\cos(\phi_1 - \phi_2) + \cos\theta_1\cos\theta_2) \tag{4.9}$$

in every coordinate system. From (4.9) we can construct a system of equations to find a third point $\mathbf{x}_3$ which is a distance $s(\mathbf{x}_3, \mathbf{x}_1) = s(\mathbf{x}_3, \mathbf{x}_2) = 1$ away from both the points $\mathbf{x}_2$ and $\mathbf{x}_3$ we

found before. While the solution cannot be written in a compact form, the system of equation turns out to be analytically solvable (the solution for $\mathbf{x}_3$ is included in the appendix in Listing B.1).

We have therefore successfully created an equilateral geodesic triangle on a sphere. However, as it turns out this method has its limits: If we tried to solve a similar system of equations as before but with the two points $\tilde{\mathbf{x}}_1 = (2\pi/5, 0)$ and $\tilde{\mathbf{x}}_2 = (2\pi/5 + 1/R, 0)$, the solutions are not analytically solvable by Mathematica. The Mathematica code for this situation can be seen in Listing B.2, where the 'Solve' command in the penultimate line yields no result. As a conclusion, this method cannot be used to generate equilateral connections/triangles for arbitrary points. As a result, it seems that due to the transcendental nature of trigonometric functions, a numerical calculation is the next plausible step.

4.1.2 Numerical solution

As a short demonstration, I show that the methods introduced in the previous chapter do indeed allow us to find a triangulation of the sphere. The solution to the system of equations generated from the geodesic distance in Eq. (4.9) can be solved by subtracting both sides and finding the roots that satisfy both expressions. An example is displayed in Fig. 4.1, where a radius of $R = 1$ was assumed. On the left the figure shows the vertices and geodesic paths of the intrinsic coordinates, while the right side shows how this triangulation actually looks like on the sphere. The python code for this calculation is presented in Listing B.3. One problem that could not be resolved in this short demonstration was that the geodesic between the points 0 and 4 could not be

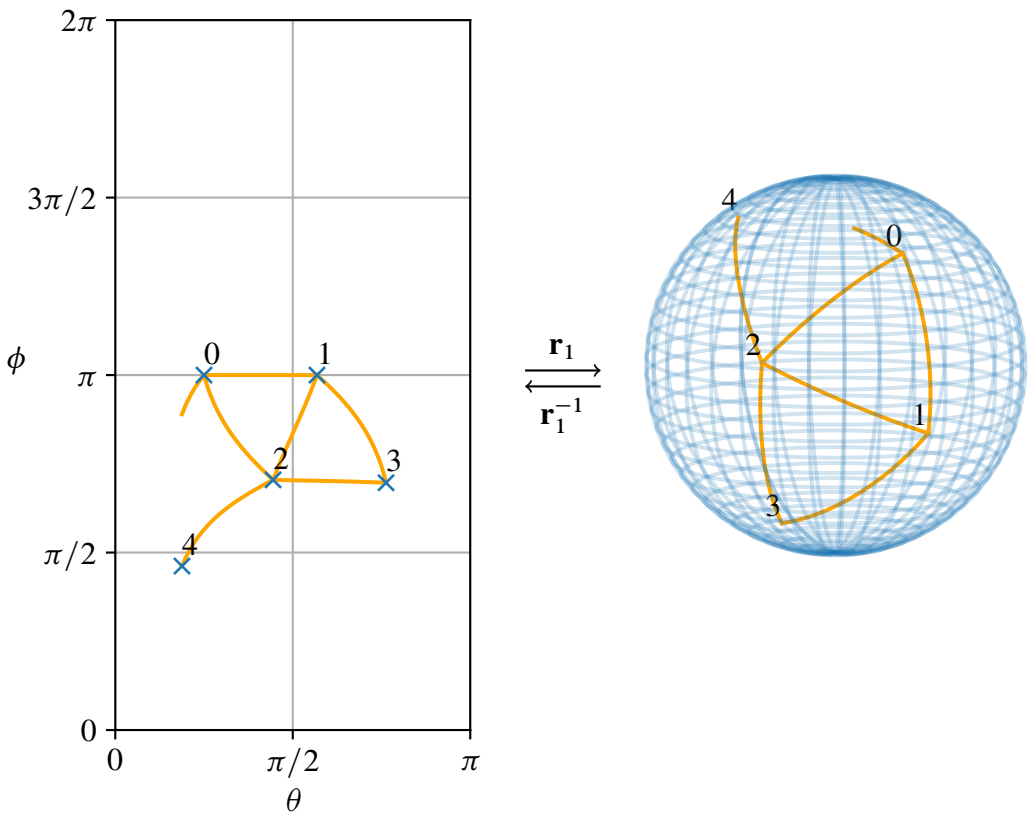

Figure 4.1: Demonstration of numerical calculations for finding geodesic triangles on a sphere. Created from Code in Listing B.3.

calculated correctly from Eq. (4.6). The difficulty probably arose because of the parametrization with θ, as the two θ coordinates lie very close. Furthermore, the triangulation process only works for a small amount of vertices, as the algorithm in which order the vertices are generated must still be improved. Nevertheless, with further investigation, the methods presented look promising in finding a successful numerical triangulation.

The implemented code works by giving two start vertices, which already have the desired separation of 1. A for-loop then iteratively generates new vertices by a root finding functions. While the order in which the vertices are generated is given by the code (which must still be improved), the start value (first guess) for finding the roots is calculated (pseudo-)randomly for each vertex. This implies that the triangulation will look different each time, but because there is a finite set of different possibilities for two given start points, one could - in theory - determine all possible triangulations for two given starting points.

4.2 Multiple coordinate systems

In addition to the coordinate system in (4.3), at least one other coordinate system is needed to construct a full atlas of the sphere. An example of an atlas would be:

$$\mathbf{r}_1(\theta_1, \phi_1) = R \begin{pmatrix} \sin\theta_1 \cos\phi_1 \\ \sin\theta_1 \sin\phi_1 \\ \cos\theta_1 \end{pmatrix}, \quad \theta_1 \in (\pi/5, 4\pi/5),\ \phi_1 \in [0, 2\pi), \tag{4.10a}$$

$$\mathbf{r}_2(\theta_2, \phi_2) = R \begin{pmatrix} \cos\theta_2 \\ \sin\theta_2 \cos\phi_2 \\ \sin\theta_2 \sin\phi_2 \end{pmatrix}, \quad \theta_2 \in (\pi/5, 4\pi/5),\ \phi_2 \in [0, 2\pi). \tag{4.10b}$$

The two coordinate systems are displayed in Fig. 4.2. The transition functions $\mathbf{r}_{12}$ and $\mathbf{r}_{21}$ can then be calculated according to (2.4):

$$\mathbf{r}_1^{-1}(x, y, z) = \left(\arccos\frac{z}{R}, \operatorname{arctan2}(x, y)\right), \tag{4.11a}$$

$$\mathbf{r}_2^{-1}(x, y, z) = \left(\arccos\frac{x}{R}, \operatorname{arctan2}(y, z)\right), \tag{4.11b}$$

$$\mathbf{r}_{12}(\theta_2, \phi_2) = \mathbf{r}_1^{-1} \circ \mathbf{r}_2 = (\arccos(\sin\theta_2 \sin\phi_2), \operatorname{arctan2}(\cos\theta_2, \sin\theta_2 \cos\phi_2)) \tag{4.11c}$$

$$\mathbf{r}_{21}(\theta_1, \phi_1) = \mathbf{r}_2^{-1} \circ \mathbf{r}_1 = (\arccos(\sin\theta_1 \cos\phi_1), \operatorname{arctan2}(\sin\theta_1 \sin\phi_1, \cos\theta_1)) \tag{4.11d}$$

We have used the function $\operatorname{arctan2}(a, b)$ instead of $\arctan(b/a)$ in order to achieve the full range of the ϕs.

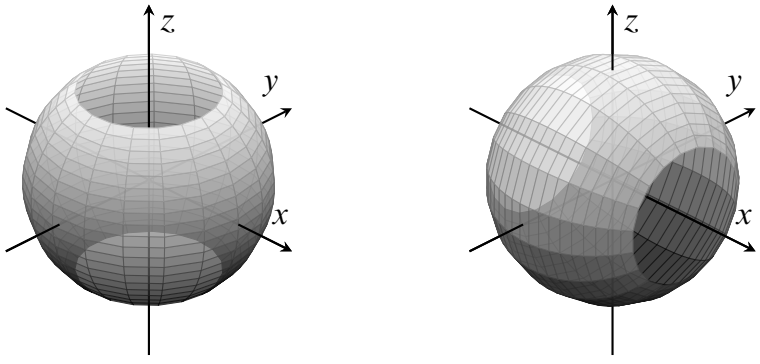

Figure 4.2: Visualization of the two coordinate systems $\mathbf{r}_1$ (left) and $\mathbf{r}_2$ (right) in Eq. (4.10).

4.2.1 Analytical solution

In the overlap regions between the two coordinate systems, Eq. (4.11c) and (4.11d) can be used to switch between the coordinates, i.e. $\mathbf{r}_{12}(\theta_2, \phi_2) = (\theta_1, \phi_1)$, $\mathbf{r}_{21}(\theta_1, \phi_1) = (\theta_2, \phi_2)$. For example, if the edge of a triangle lies inside the overlap region, there is no difficulty in then switching coordinates, before continuing the triangulation process. However, as mentioned before, solving this analytically was found to not be possible with the methods used before.

When creating a geodesic triangle given two already existing points on the manifold, there are three different cases that can occur at the boundaries between two coordinate systems, when the third point completing the triangle can only be put into the image of the second coordinate system $\mathbf{r}_2$, and can therefore not be represented by $\mathbf{r}_1$:

[Case 1] Both vertices lie on the overlap of the two coordinate systems.

[Case 2] One of the existing vertices only lies inside the image of $\mathbf{r}_1$, while the other lies on the overlap of the two coordinate systems.

[Case 3] Both of the two existing vertices lie solely in the image of $\mathbf{r}_1$.

Case 1 is the easiest to handle, as we can simply switch to the coordinates of the second coordinate system with the help of the transition function $\mathbf{r}_{21}$ in (4.11d) and continue to build more vertices from there. Cases 2 and 3 impose a greater challenge, as for the point which does not lie inside the overlap, it is necessary to calculate the geodesic distance up to a (variable) point in the overlap, use $\mathbf{r}_{21}$ to switch coordinates, and then continue the measuring of geodesic distance from there. As an example for case 3, let $\mathbf{x}_1, \mathbf{x}_2$ be two points solely represented by $\mathbf{r}_1$ with a geodesic distance of 1 between them and let $\mathbf{x}_{\text{mid},1}, \mathbf{x}_{\text{mid},2}$ be two point in the overlap region. If the edge of $\mathbf{r}_1$'s domain lies inside the overlap, one could for example limit the variability of the two mid-points to lie along this edge, rather than anywhere inside the region of overlap. Using Eq. (4.9) and (4.11), the equations which have to be satisfied to find the third point $\mathbf{x}_3$ which is solely represented by $\mathbf{r}_2$ are

$$
\begin{aligned}
s(\mathbf{r}_1^{-1}(\mathbf{x}_1), \mathbf{r}_1^{-1}(\mathbf{x}_{\text{mid},1})) + s(\mathbf{r}_2^{-1}(\mathbf{x}_{\text{mid},1}), \mathbf{r}_2^{-1}(\mathbf{x}_3)) &= 1, \\
s(\mathbf{r}_1^{-1}(\mathbf{x}_2), \mathbf{r}_1^{-1}(\mathbf{x}_{\text{mid},2})) + s(\mathbf{r}_2^{-1}(\mathbf{x}_{\text{mid},2}), \mathbf{r}_2^{-1}(\mathbf{x}_3)) &= 1.
\end{aligned}
$$

However, this is a system of 2 equations with 4 unknowns. Two further constraints are that the geodesics do indeed continue geodetically after the mid-points, i.e. that there is no 'bend' at the mid-points.

Nevertheless, one could avoid case 2 and 3 by making the overlap region wide enough, or reducing the edge length (since we would do so anyway in the limit) so that at least one edge must *always* be inside it. As mentioned before, in this case one only has to apply the transition functions in Eq. (4.11) (for the case of a sphere).

4.2.2 Qualitative methods

Suppose we can calculate the geodesic $(\theta(\lambda), \phi(\lambda))$ connecting two arbitrary points $\mathbf{x}_1, \mathbf{x}_2$ from the same coordinate system and suppose that we can calculate the distance arbitrarily through the action $d(\mathbf{x}_1, \mathbf{x}_2)$. If we look at case 3 from before (see Fig. 4.3), we can calculate every geodesic starting at point $\mathbf{A}$, going through an arbitrary mid-point $\mathbf{A}' \in \mathbf{r}_1(U_1) \cap \mathbf{r}_2(U_2)$, translating this geodesic into the second coordinate system with $\mathbf{r}_{21}$, which we can use to extend the geodesic, and then ending on the point $\mathbf{C}$ so that the total geodesic length is 1. Iterating this process for *every* mid-point in $\mathbf{r}_1(U_1) \cap \mathbf{r}_2(U_2)$ leads to a set of points $\mathcal{C}_A$. Repeating this method for the second point $\mathbf{B}$ from $\mathbf{r}_1$, one gets the set $\mathcal{C}_B$. The desired point is then (unique, at least for the

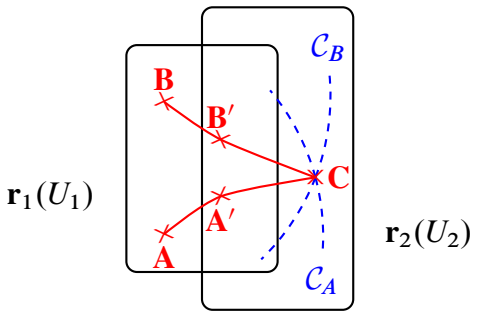

Figure 4.3: Qualitative view of finding the third vertex **C** in the second coordinate system.

sphere) $\mathbf{C} \in \mathcal{C}_A \cap \mathcal{C}_B$ (see Fig. 4.3). However, this method is quite 'brute force', which would make numerical computation perhaps expensive.

To find a more elegant expression, we first consider splitting up the action at a point $\mathbf{x}(\lambda_{\text{mid}})$, which lies inside the overlap. For the second integral we then may use the transition function $\mathbf{r}_{21}$ from (4.11d):

$$d(\mathbf{A},\mathbf{B}) = \int_{\mathbf{A}}^{\mathbf{B}} ds = \int_{\lambda_0}^{\lambda_{\text{mid}}} \sqrt{g_{\mu\nu}\frac{\partial x^\mu}{\partial\lambda}\frac{\partial x^\nu}{\partial\lambda}}\,d\lambda + \int_{\lambda_{\text{mid}}}^{\lambda_{\text{end}}} \sqrt{g_{\mu\nu}\frac{\partial r_{21}^\mu}{\partial\lambda}\frac{\partial r_{21}^\nu}{\partial\lambda}}\,d\lambda \stackrel{!}{=} 1 \tag{4.13}$$

However, it might be appropriate at this point to check if such an 'extension' of a geodesic is possible for the coordinate systems used in this chapter. Let us consider a simple geodesic described by the first coordinate system in (4.3): $(x_1^i(\lambda)) = (\pi/2-\lambda, 0)$, where $\lambda \in (0, 3\pi/10)$ and the bounds come from the domain of the first system. We will label the start of this curve as $A = x_1(\pi/5)$. Translating this geodesic to the second coordinate system, one gets:

$$(r_{21}^i(\lambda, 0)) = (\arccos[\sin(\pi/2-\lambda)], \arctan2[0, \cos(\pi/2-\lambda)]) = (\lambda, 0) = (x_2^i(\lambda)), \tag{4.14}$$

where we already know that this is indeed a geodesic, i.e. the equator of the second coordinate system. The expression is therefore valid for $\lambda \in (\pi/5, 4\pi/5)$ for the second coordinate system and we will set the end point at $\mathbf{B} = x_2(4\pi/5)$. We therefore have a geodesic defined for $\lambda \in (0, 4\pi/5)$ where $\lambda \in (0, 3\pi/10)$ is defined in the first coordinate system and $\lambda \in (\pi/5, 4\pi/5)$ is defined in the second coordinate system. Therefore, the overlap of the geodesic, where it is defined in both coordinate system, lies in $\lambda \in (\pi/5, 3\pi/10)$. Choosing $\lambda_{\text{mid}} = \pi/4$ in the overlap region, we can use Eq. (4.13) to calculate the length of this geodesic.

$$d(\mathbf{A},\mathbf{B}) = R\int_{\pi/5}^{\pi/4} d\lambda + R\int_{\pi/4}^{4\pi/5} d\lambda = R\frac{3\pi}{5}, \tag{4.15}$$

which is of course what we would expect.

4.2.3 Testing the limits

We are now interested in what might happen if we calculate the distance similarly as in Eq. (4.13) while this time not being so careful and neglecting the domain of the first coordinate system. The restraint in the domain of θ_1 in Eq. (4.10) was set arbitrarily to $(\pi/5, 4\pi/5)$ just so we cut out the singularities (which are ill-defined) at $\theta_1 \in \{0, \pi\}$. Therefore, it is of interest to test what happens in the integral of $d(\mathbf{A},\mathbf{B})$ if we, for example, integrate over this singularity, using the same geodesic as before, i.e. $\mathbf{x}_1(\lambda) = (\pi/2-\lambda, 0)$, however where this time we stay in this coordinate system and integrate in $\lambda \in (\pi/5, 4\pi/5)$. This is trivial however, as we already know that the integrand of this geodesic is 1 and we get exactly the same result as in Eq. (4.15).

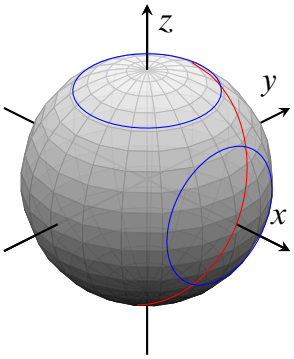

Figure 4.4: Example path (red) to test integrating over a coordinate singularity. Bounds of coordinate systems indicated in blue.

As a second test, let us look at a geodesic calculated from Eq. (4.6) of the form $\mathbf{x}_1(\lambda) = (\lambda, \phi(\lambda))$, where we labelled λ as the parameter instead of θ. Experimenting with different values of the general solution lead to the following geodesic (in $\mathbf{r}_1$):

$$\phi_1(\lambda) = \cos^{-1}\left(\frac{\cot\lambda}{C_1}\right) + C_2, \quad \text{with} \quad C_1 = -\sqrt{3},\ C_2 = \frac{3\pi}{2}, \tag{4.16}$$

which is of course only valid in $\mathbf{r}_1$ for $\lambda \in (\pi/5, 4\pi/5)$. We could technically now extend this interval in order to achieve a similar situation as before, where a part of the curve is only valid in $\mathbf{r}_1$, one in the overlap, and one only valid in $\mathbf{r}_2$ (as depicted in Fig. 4.4) However, we are now only interested in the part of $d(\mathbf{A}, \mathbf{B})$, where we are integrating over the singularity of $\mathbf{r}_2$, which lies in $\mathbf{r}_1(\pi/2, 0)$.

Inserting the expression for ϕ' in Eq. (4.5b) into the expression for $d(\mathbf{A}, \mathbf{B})$ in Eq. (4.4) we get

$$\Delta s = \int \sqrt{1 + \frac{C^2}{\sin^2\theta - C^2}}\, d\theta = \int \frac{|\sin\theta|}{\sqrt{\sin^2\theta - C^2}}\, d\theta, \tag{4.17}$$

which can be solved as demonstrated in Eq. (A.2) in the appendix.

We can now compare the two methods of calculating the length: Let us consider the same path (4.16) but this time for $\lambda \in (2\pi/5, 3\pi/5)$. For $\lambda = \pi/2$ we get from Eq. (4.16):

$$\phi_1\left(\frac{\pi}{2}\right) = 2\pi \equiv 0, \tag{4.18}$$

which is exactly one of the singularities of $\mathbf{r}_2$. As a reference, integrating over this in $\mathbf{r}_1$ gives us, from Eqs. (4.17), (A.2) with $C = (C_1^2 + 1)^{-1/2} = 1/2$:

$$\begin{aligned} d(\mathbf{A}, \mathbf{B}) &= \int_{2\pi/5}^{3\pi/5} \frac{|\sin\theta|}{\sqrt{\sin^2\theta - 1/4}}\, d\theta = \int_{2\pi/5}^{3\pi/5} \frac{\sin\theta}{\sqrt{\sin^2\theta - 1/4}}\, d\theta = \\ &\overset{(A.2)}{=} \arccos\left(\frac{2\cos\left(\frac{3\pi}{5}\right)}{\sqrt{3}}\right) - \arccos\left(\frac{2\cos\left(\frac{2\pi}{5}\right)}{\sqrt{3}}\right) \approx 0.73. \end{aligned} \tag{4.19}$$

Now let us compare this to the calculation in $\mathbf{r}_2$. We first have to use the transition function $\mathbf{r}_{21}$ in Eq. (4.11d) and then of course ignore the bounds of $\mathbf{r}_2$ and let $\theta_2 \in [0, \pi]$. This can be

most easily calculated in Mathematica (see Listing B.4). We end up at:

$$\begin{aligned}\mathbf{r}_{21}(\lambda, \phi_1(\lambda)) &= (\theta_2(\lambda), \phi_2(\lambda)) = \\ &= \left(\arccos\left(\sin\lambda \sqrt{1 - \frac{\cot^2\lambda}{3}} \right),\ \operatorname{arctan2}\left(\frac{\cos\lambda}{\sqrt{3}}, \cos\lambda \right) \right) = \\ &= \left(\arccos\left(\sin\lambda \sqrt{1 - \frac{\cot^2\lambda}{3}} \right),\ \frac{\pi}{3} \right).\end{aligned} \tag{4.20}$$

The constant value in ϕ_2 is exactly what we would expect for a geodesic in $\mathbf{r}_2$ going through the poles. Consequently, $d\phi_2/d\lambda = 0$ and

$$\frac{d\theta_2}{d\lambda} = -\frac{2|\cos\lambda| \sec\lambda}{\sqrt{3 - \cot^2\lambda}}, \tag{4.21}$$

which was again calculated with Mathematica (see Listing B.4). Now, calculating the geodesic length in $\mathbf{r}_2$ we get:

$$\begin{aligned}d(\mathbf{A}, \mathbf{B}) &= \int_{2\pi/5}^{3\pi/5} \sqrt{g_{\mu\nu} \frac{\partial x^\mu}{\partial\lambda} \frac{\partial x^\nu}{\partial\lambda}}\, d\lambda = \int_{2\pi/5}^{3\pi/5} \left| \frac{2\cos\lambda \sec\lambda}{\sqrt{3 - \cot^2\lambda}} \right| d\lambda = \\ &= \int_{2\pi/5}^{3\pi/5} \frac{2}{\sqrt{3 - \cot^2\lambda}}\, d\lambda = \\ &\overset{(A.3)}{=} \arctan\left(\frac{2\cot\left(\frac{2\pi}{5}\right)}{\sqrt{3 - \cot^2\left(\frac{3\pi}{5}\right)}} \right) - \arctan\left(\frac{2\cot\left(\frac{2\pi}{5}\right)}{\sqrt{3 - \cot^2\left(\frac{3\pi}{5}\right)}} \right) \approx 0.73,\end{aligned} \tag{4.22}$$

which is exactly the same result as when integrated in $\mathbf{r}_1$ in Eq. (4.19). The solution to the integral is derived in the appendix in Eq. (A.3).

5 Schwarzschild geometry

One solution to the vacuum Einstein field equation describes the curvature of spacetime around a non-rotating spherically symmetrical massive object, like stars or even black holes [12]. It is called the Schwarzschild geometry and when described by Schwarzschild coordinates, the line element is given by

$$ds^2 = -\left(1 - \frac{2M}{r}\right) dt^2 + \left(1 - \frac{2M}{r}\right)^{-1} dr^2 + r^2(d\theta^2 + \sin^2\theta\, d\phi^2) \tag{5.1}$$

in geometrized units [3]. Therefore, the Schwarzschild metric reads

$$(g_{\alpha\beta}) = \operatorname{diag}[-(1 - 2M/r), (1 - 2M/r)^{-1}, r^2, r^2 \sin^2\theta], \tag{5.2}$$

where the coordinates are labelled with (t, r, θ, ϕ). M is the total mass of the spherical object located at the centre. Furthermore, there are coordinate singularities at the Schwarzschild radius $r_S = 2M$ (which is $r_S = 2GM/c^2$ in non-geometrized units) and at $r = 0$. For normal stars the Schwarzschild radius is much smaller than their actual radius, which is why we will be looking at the geometry of a Schwarzschild black hole.

The conserved quantities, which arise from the independence of t and ϕ in (5.1) are labelled with [3]:

$$e \equiv \left(1 - \frac{2M}{r}\right)\frac{dt}{d\tau}, \tag{5.3a}$$

$$\ell \equiv r^2 \sin^2\theta \, \frac{d\phi}{d\tau}. \tag{5.3b}$$

In the non-relativistic limit, these conservations are identified with the conservation of energy (e) and angular momentum (ℓ). Because of the spherical symmetry, it becomes clear that the particle orbits are not leaving a certain spacial plane and one can set $\theta = \pi/2$, $d\theta = 0$ for simplicity, similarly on how one shows that the equator is a geodesic of the 2-sphere. If we define

$$\mathcal{E} \equiv (e^2 - 1)/2$$

$$V_{\text{eff}}(r) \equiv -\frac{M}{r} + \frac{\ell^2}{2r^2} - \frac{M\ell^2}{r^3},$$

the geodesic equation is reduced to a differential equation of the radius [3]:

$$\mathcal{E} = \frac{1}{2}\left(\frac{dr}{d\tau}\right)^2 + V_{\text{eff}}(r). \tag{5.4}$$

Due to the singularities at the Schwarzschild radius and at the origin, the Schwarzschild coordinates are only valid in $r \in (2M, \infty)$ [12]. To describe the spacetime beyond that, other coordinates are needed. By a coordinate transformation to *Kruskal-Szekeres* (or simply Kruskal) coordinates, the Schwarzschild metric (5.1) becomes [3]:

$$ds^2 = \frac{32M^3}{r} e^{-r/2M}\left(-dV^2 + dU^2\right) + r^2(d\theta^2 + \sin^2\theta \, d\phi^2), \tag{5.5}$$

where the coordinates are labelled with (V, U, θ, ϕ). r, θ and ϕ are the same as in the Schwarzschild coordinates, while V and U are defined as [3]:

$$V = \begin{cases} \sqrt{\frac{r}{2M} - 1}\, e^{r/4M} \sinh\left(\frac{t}{4M}\right), & r \geq 2M \\ \sqrt{1 - \frac{r}{2M}}\, e^{r/4M} \cosh\left(\frac{t}{4M}\right), & r < 2M \end{cases}, \tag{5.6a}$$

$$U = \begin{cases} \sqrt{\frac{r}{2M} - 1}\, e^{r/4M} \cosh\left(\frac{t}{4M}\right), & r \geq 2M \\ \sqrt{1 - \frac{r}{2M}}\, e^{r/4M} \sinh\left(\frac{t}{4M}\right), & r < 2M \end{cases}. \tag{5.6b}$$

We are now interested in the overlap between Schwarzschild and Kruskal coordinates in the interval $r \in (2M, 4M) = (r_S, 2r_S)$. We therefore only consider the definitions of U and V for $r \geq 2M$. In this overlap the transition functions become:

$$\mathbf{r}_{21}(t, r, \theta, \phi) = (U(t, r), V(t, r), \theta, \phi), \tag{5.7a}$$

$$\mathbf{r}_{12}(V, U, \theta, \phi) = \left(2M\left[1 + W_0\left(\frac{U^2 - V^2}{e}\right)\right], 4M \operatorname{artanh}(V/U), \theta, \phi\right), \tag{5.7b}$$

with U, V defined as above for $r \geq 2M$ and where W_0 is the Lambert W function as a solution for r of the implicit equation [3]:

$$\left(\frac{r}{2M} - 1\right) e^{r/2M} = U^2 - V^2 \,. \tag{5.8}$$

5.1 Radial plunge

By setting $\ell = 0$ (or $d\phi = 0$), we will expect a path drifting inwards. If we give the test particle a kinetic energy of 0 at $r \to \infty$, we see that $e = 1$ and therefore $\mathcal{E} = 0$. Equation (5.4) can then be easily solved, which Hartle demonstrates in [3]:

$$\frac{dr}{d\tau} = \pm\sqrt{\frac{2M}{r}}, \tag{5.9a}$$

$$r(\tau) = \left(\frac{3}{2}\right)^{2/3} (2M)^{1/3}(\tau - \tau_0)^{2/3}, \tag{5.9b}$$

$$\frac{dt}{d\tau} = \frac{1}{1 - 2M/r}, \tag{5.9c}$$

$$t(\tau) = t_0 + 2M\left[-\frac{2}{3}\left(\frac{r}{2M}\right)^{3/2} - 2\left(\frac{r}{2M}\right)^{1/2} + \ln\left|\frac{(r/2M)^{1/2}+1}{(r/2M)^{1/2}-1}\right|\right], \tag{5.9d}$$

where the negative square root in (5.9a) corresponds to a path going inward. We are now, again, interested in the geodesic equation. We want to set up a path that crosses the singularity of the Schwarzschild coordinates at $r_S = 2M$. As the Lagrangian is a constant of motion in GR (for natural parametrizations), we would get $\Delta\tau = 1$, which is of course what we would expect, since $\Delta\tau$ *is* the 'distance' between two time-like separated points.

However, since we are interested to see what might happen in the integral when we cross r_S, we could substitute $r(\tau)$ with $d\tau = \sqrt{r/2M}\, dr$. We then see immediately that the integrand is still continuous and well-defined for $r > 0$, in contrast to the coordinate time t, which diverges. This shows that the singularity at r_S is purely a coordinate artifact of the Schwarzschild coordinates, and could therefore be extended to $r < r_S$ when using Kruskal coordinates.

Calculation in Kruskal coordinates

We now perform the analogous calculation for the radial plunge, but now in Kruskal coordinates. The line element is given by Eq. (5.5). For a timelike geodesic, $d\tau^2 = -ds^2$, we get for the radial path ($d\theta = d\phi = 0$):

$$d\tau^2 = \frac{32M^3}{r} e^{-r/2M}\left(dV^2 - dU^2\right).$$

If we assume parametrization with r, we get:

$$d\tau = \sqrt{\frac{32M^3}{r} e^{-r/2M}\left(\left(\frac{dV}{dr}\right)^2 - \left(\frac{dU}{dr}\right)^2\right)}\, dr. \tag{5.10}$$

To compute the derivatives $\frac{dU}{dr}$ and $\frac{dV}{dr}$, we can make use of the chain rule, i.e. $\frac{dV}{dr} = \frac{\partial V}{\partial r} + \frac{\partial V}{\partial t}\frac{dt}{dr}$. From Eq. (5.9a) and (5.9c), we get:

$$\frac{dt}{dr} = \frac{dt/d\tau}{dr/d\tau} = \frac{\sqrt{r/2M}}{1 - 2M/r}.$$

The partial derivatives of the Kruskal coordinates (V, U) with respect to the Schwarzschild coordinates (t, r) must be calculated from their definitions in Eq. (5.6a) and (5.6b). For $r > 2M$, the partial derivatives are:

$$\frac{\partial V}{\partial t} = \frac{U}{4M}, \qquad \frac{\partial V}{\partial r} = \frac{rV}{8M^2(r/2M - 1)},$$
$$\frac{\partial U}{\partial t} = \frac{V}{4M}, \qquad \frac{\partial U}{\partial r} = \frac{rU}{8M^2(r/2M - 1)}.$$

Substituting these into Eq. 5.10 gives

$$d\tau = -\sqrt{\frac{r}{2M}}\, dr \ ,$$

as before.

This showed that the integrand for the proper time is identical in both coordinate systems, and is smoothly calculable across r_S, just as the length of a geodesic on a sphere was shown to be smoothly calculable across the boundary of two coordinate systems in its atlas.

5.2 Geodesic with angular momentum

From Eq. (2.12) we can calculate the Christoffel symbols for the Schwarzschild metric in (5.2). Since the metric is diagonal, we have $g^{\alpha\alpha} = 1/g_{\alpha\alpha}$. We therefore get:

$$\begin{aligned}
\Gamma^0_{01} &= \Gamma^0_{10} = \frac{M}{r^2 - 2Mr}, & & \\
\Gamma^1_{00} &= \frac{M}{r^2}(1 - 2M/r), & \Gamma^1_{11} &= -\frac{M}{r^2 - 2Mr}, \\
\Gamma^1_{22} &= 2M - r, & \Gamma^1_{33} &= (2M - r)\sin^2\theta, \\
\Gamma^2_{12} &= \Gamma^2_{21} = \frac{1}{r}, & \Gamma^2_{33} &= -\sin\theta\cos\theta, \\
\Gamma^3_{13} &= \Gamma^3_{31} = \frac{1}{r}, & \Gamma^3_{23} &= \Gamma^3_{32} = \cot\theta \ .
\end{aligned} \tag{5.12}$$

From Eq. (2.11) we would get the geodesic equations. However, as we already discussed, we can set $\theta = \pi/2$. The equation we get for r (were we use $u^\alpha = dx^\alpha/d\tau$):

$$\frac{du^1}{d\tau} + \frac{M}{r^2}(1 - 2M/r)(u^0)^2 - \frac{M}{r^2 - 2Mr}(u^1)^2 - (r - 2M)(u^2)^2 - (r - 2M)\sin^2\theta(u^3)^2 = 0$$

can be replaced by the norm of the four-velocity:

$$g_{\mu\nu}u^\mu u^\nu = -(1-2M/r)(u^0)^2 + \frac{1}{1-2M/r}(u^1)^2 + r^2(u^3)^2 = \begin{cases} -1 & \text{if timelike} \\ 1 & \text{if spacelike} \end{cases} \tag{5.13}$$

since differentiating with respect to τ and inserting the geodesic equations of the other components recovers the geodesic equation for the radius. This way we can choose between timelike and spacelike geodesics, which of course is needed for CDT. We get the following set of equations:

$$\frac{d^2t}{d\tau^2} = -\frac{2M}{r^2 - 2Mr}\frac{dr}{d\tau}\frac{dt}{d\tau}, \tag{5.14a}$$

$$\frac{d^2\phi}{d\tau^2} = -\frac{2}{r}\frac{dr}{d\tau}\frac{d\phi}{d\tau} \tag{5.14b}$$

$$-\left(1 - \frac{2M}{r}\right)^{-1} e^2 + \left(1 - \frac{2M}{r}\right)^{-1}\left(\frac{dr}{d\tau}\right)^2 + r^2\left(\frac{d\phi}{d\tau}\right)^2 = \begin{cases} -1 & \text{if timelike} \\ 1 & \text{if spacelike} \end{cases}. \tag{5.14c}$$

5.2.1 Triangulation in the r-t-plane

For a timelike radial plunge, with arbitrary constant e, the equation for dt/dr from Eq. (5.9) becomes:

$$\frac{dt}{dr} = \frac{e}{1 - 2M/r}\frac{-1}{\sqrt{2(\mathcal{E} + M/r)}}. \tag{5.15}$$

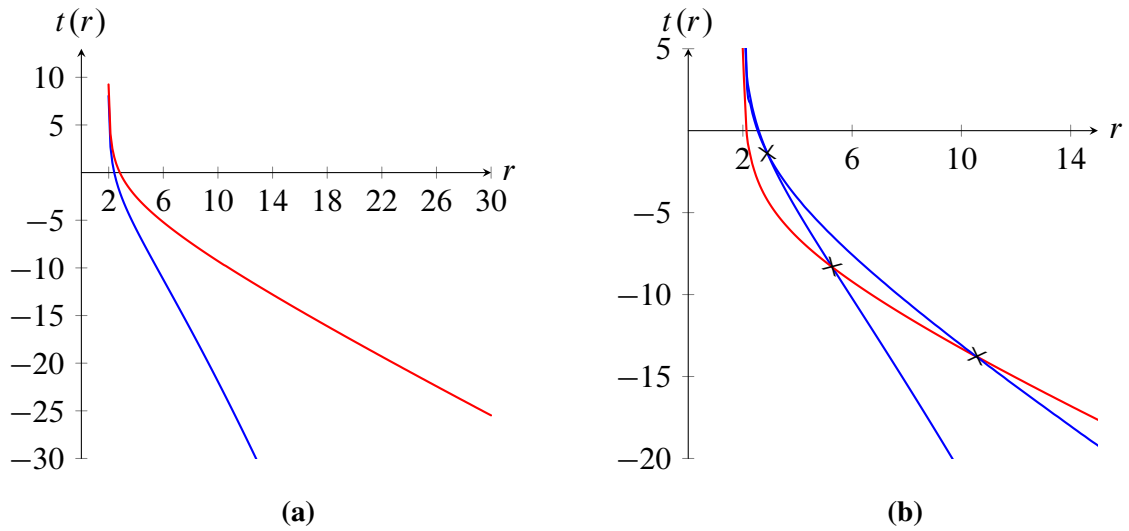

Figure 5.1: (**a**) Geodesics $t(r)$ of the Schwarzschild metric. (**b**) Geodesic triangle, where the $\times$ indicate vertices. Blue: timelike. Red: spacelike.

Turning to spacelike radial geodesics, we get from Eq. (5.14c):

$$-\left(1-\frac{2M}{r}\right)^{-1}e^2+\left(1-\frac{2M}{r}\right)^{-1}\left(\frac{dr}{d\tau}\right)^2=1, \tag{5.16}$$

which can be rewritten as

$$\underbrace{\frac{1}{2}(e^2+1)}_{\equiv\tilde{\mathcal{E}}}=\frac{1}{2}\left(\frac{dr}{d\tau}\right)^2-V_{\text{eff}}(r),\quad V_{\text{eff}}(r)=-\frac{M}{R}\quad\text{(for radial plunge).} \tag{5.17}$$

Replacing now $d\tau\to ds$, we get:

$$\left(\frac{dr}{ds}\right)^2=2\tilde{\mathcal{E}}-2M/r\implies\frac{dr}{ds}=\pm\sqrt{2(\tilde{\mathcal{E}}-2M/r)}, \tag{5.18a}$$

$$\frac{dt}{ds}=\frac{e}{1-2M/r}, \tag{5.18b}$$

$$\implies\frac{dt}{dr}=\frac{dt/ds}{dr/ds}=\frac{e}{1-2M/r}\frac{1}{\pm\sqrt{2(\tilde{\mathcal{E}}-M/r)}}. \tag{5.18c}$$

Mathematica's symbolic integrator seemed to only return solutions involving complex values that could not be easily simplified to a real form. In the end, GeoGebra was used to get a sensible solution for both the timelike and spacelike geodesics $t(r)$ for $M=e=1$:

$$\text{timelike:}\quad t(r)=-2\ln\left(\left|2\sqrt{r}-2\sqrt{2}\right|\frac{-\sqrt{r}+\sqrt{2}}{-2r+4}\right)-\frac{\sqrt{2}}{3}r^{3/2}-2\sqrt{2r}+C, \tag{5.19a}$$

$$\begin{aligned}\text{spacelike:}\quad t(r)=&\frac{5}{2\sqrt{2}}\ln\left|-2r+2\sqrt{r^2-r}+1\right|+2\ln\left(-2\sqrt{2}+3\right)\\&-2\ln\left|1-\frac{2\sqrt{2}}{-r+\sqrt{r^2-r}+\sqrt{2}+2}\right|-\sqrt{\frac{r^2-r}{2}}+C.\end{aligned} \tag{5.19b}$$

The geodesics are visualized in Fig. 5.1a, where the coordinate singularity at $r = 2$ is immediately noticeable. Testing around with the solution, we find that the graphs come closer together for increasing values of e. The triangulation process then consists of splitting up the geodesics into slices $r_i = r(\tau_i)$, where $\tau_i = \tau_0 + n$ with $n \in \mathbb{N}$. The time coordinates are then determined by (5.19). We would then have to find more geodesics with different values of e and integration constants and connect them to find triangles with two timelike and a spacelike connection. This is demonstrated by the triangle in Fig. 5.1b, which are however not equilateral, because of problems with Mathematica.

6 Conclusion and outlook

As we have seen in Chapter 3, the implementation of a triangulated 2-D Minkowski space has worked as intended, also showing how different realizations of the triangulation could look like (see Fig. 3.2).

The analysis of the 2-sphere proved to be more difficult, due to the transcendental nature of the systems of equations encountered. Nonetheless, we were able to show methods to produce equilateral geodesic triangles both analytically and numerically (see Fig. 4.1). Furthermore, we demonstrated how one could calculate transition functions in multiple coordinate systems and provided examples that the geodesic integral did not diverge at coordinate singularities. Nevertheless, we could not provide robust methods in triangulating the whole surface of the 2-sphere, neither analytically nor numerically. While the numeric demonstration could be improved by more robust methods, such as a different parametrization of the geodesics, the analytical approach in this thesis was limited by Mathematica's abilities to solve the arising equations.

For the Schwarzschild geometry, we demonstrated how to calculate timelike and spacelike geodesics. We showed how an atlas can be constructed with a combination of Schwarzschild and Kruskal-Szekeres coordinates and confirmed that the coordinate singularity of the Schwarzschild coordinates at $r = 2M$ had no impact on the geodesic integral. Although analytical expressions for spacelike and timelike geodesics were found, a full triangulation of the Schwarzschild geometry was not carried out. This was due to the problem encountered in Mathematica with the geodesic integrals of Eq. (5.15) for the timelike and (5.18c) for the spacelike geodesic. However, the methods for achieving such a triangulation were briefly discussed, and an example triangle was presented in Fig. 5.1b. Since the issue with Mathematica could not be resolved within the scope of this thesis, it remains a subject for future investigation.

References

[1] L. W. Würger, *Extraction of the metric within the framework of Causal Dynamical Triangulation*, 2024, https://static.uni-graz.at/fileadmin/_Persoenliche_Webseite/maas_axel/wuerger_bachelor.pdf (visited on 10/07/2025).

[2] C. Perner, *Metric reconstruction with causal dynamical triangulation*, 2023, https://static.uni-graz.at/fileadmin/_Persoenliche_Webseite/maas_axel/Bachelorarbeit_Metric_reconstruction_with_causal_dynamical_triangulation_Christina_Perner.pdf (visited on 10/07/2025).

[3] J. B. Hartle, *Gravity: An Introduction to Einstein's General Relativity* (Cambridge University Press, Cambridge, 2021).

[4] R. Sharipov, *Quick introduction to tensor analysis*, 2004, arXiv:math/0403252 [math.HO].

[5] S. M. Carroll, *Spacetime and Geometry: An Introduction to General Relativity* (Cambridge University Press, 2019).

[6] M. Nakahara, *Geometry, topology and physics* (CRC press, 2018).

[7] B. Felsager, *Geometry, particles, and fields* (Springer-Verlag, 1998).

[8] A. Forcier, *Introductory Causal Dynamical Triangulation*, 2011, arXiv:1109.3879 [hep-th].

[9] R. Loll, *Quantum Curvature as Key to the Quantum Universe*, 2023, arXiv:2306.13782 [gr-qc].

[10] R. Loll, J. Ambjorn and J. Jurkiewicz, *The Universe from Scratch*, 2006, arXiv:0509010 [hep-th].

[11] Wikimedia Commons contributors, *Radiobservatório do Itapetinga*, 2020, https://commons.wikimedia.org/w/index.php?title=File:Radiobservat%C3%B3rio_do_Itapetinga_(May_2018)_01.jpg&oldid=505372649 (visited on 14/01/2025).

[12] D. Tong, *General Relativity*, 2019, https://www.damtp.cam.ac.uk/user/tong/gr/gr.pdf (visited on 05/05/2025).

A Integrals

$$
\begin{aligned}
I_1 &= \int \frac{C}{\sin\theta\sqrt{\sin^2\theta - C^2}}\,d\theta = \int \frac{C\csc^2\theta}{\sqrt{1 - C^2\csc^2\theta}}\,d\theta = \\
&= \left|\begin{matrix} u = \cot\theta, \\ du = -\csc^2\theta\,d\theta = -(u^2+1)\,d\theta \end{matrix}\right| = \\
&= -\int \frac{C}{\sqrt{1 - C^2(u^2+1)}}\,du = -\int \frac{1}{\sqrt{C_1^2 - u^2}}\,du = \\
&= -\arccos\left(\frac{u}{C_1}\right) + \text{const.} = \\
&= -\arccos\left(\frac{\cot\theta}{C_1}\right) + \text{const.} \qquad \left(C_1 = \sqrt{\frac{1}{C^2} - 1},\ C \in \mathbb{R},\ |C| < 1\right).
\end{aligned}
\tag{A.1}
$$

$$
\begin{aligned}
I_2 &= \int \frac{\sin\theta}{\sqrt{\sin^2\theta - C^2}}\,d\theta = \int \frac{\sin\theta}{\sqrt{1 - C^2 - \cos^2\theta}}\,d\theta = \left|\begin{matrix} u = \cos\theta, \\ du = -\sin\theta\,d\theta \end{matrix}\right| = \\
&= -\int \frac{1}{\sqrt{1 - C^2 - u^2}}\,du = -\frac{1}{\sqrt{1-C^2}}\int \frac{1}{\sqrt{1 - \frac{u^2}{1-C^2}}}\,du = \\
&= \arccos\left(\frac{u}{\sqrt{1-C^2}}\right) + \text{const.} = \\
&= \arccos\left(\frac{\cos\theta}{\sqrt{1-C^2}}\right) + \text{const.} \qquad (C \in \mathbb{R},\ |C| < 1).
\end{aligned}
\tag{A.2}
$$

$$
\begin{aligned}
I_3 &= \int \frac{2}{\sqrt{3 - \cot^2\lambda}}\,d\lambda = \left|\begin{matrix} u = \cot\lambda, \\ du = -\csc\lambda\,d\lambda \\ = -(u^2+1)\,d\lambda \end{matrix}\right| = \\
&= -2\int \frac{1}{\sqrt{3 - u^2}(u^2+1)}\,du = \left|\begin{matrix} t = \sqrt{3}\sin t, \\ du = \sqrt{3}\cos t\,dt \end{matrix}\right| = \\
&= -2\int \frac{1}{3\sin^2 t + 1}\,dt = \left|\begin{matrix} v = \tan t, \\ dv = (1+v^2)\,dt, \\ \sin^2 t = \frac{v^2}{v^2+1} \end{matrix}\right| = -2\int \frac{1}{4v^2+1}\,dv = \\
&= -\arctan(2v) + \text{const.} = \\
&= -\arctan\left(\frac{2\cot\lambda}{\sqrt{3 - \cot^2\lambda}}\right) + \text{const.} \qquad (\lambda \in (\pi/6, 5\pi/6)).
\end{aligned}
\tag{A.3}
$$

B Code

Listing B.1: Mathematica code for successful analytical calculation of geodesic triangle and unsuccessful calculation for the parametrization between two vertices.

```
In[73]:= (* \
    define function for geodesic distance from the central angle *)
    geodesicDistance[R_, \[Theta]1_, \[Phi]1_, \[Theta]2_, \[Phi]2_] :=
      R *ArcCos[
        Sin[\[Theta]1] Sin[\[Theta]2] Cos[\[Phi]1 - \[Phi]2] +
         Cos[\[Theta]1] Cos[\[Theta]2]];
```

```
    Clear[R]
    (*R = 1*)

    {theta1, phi1} = {Pi/2, 0}; (* define starting point *)
    phi2 = 0; (* constraint for second point *)
    sol2 = Simplify[
        SolveValues[geodesicDistance[R, theta1, phi1, x, phi2] == 1, x],
        Assumptions -> 1/Pi < R] /. C[1] -> 0 ;
    theta2 = sol2[[1]]
    N[%] /. R -> 1

    sol3 = FullSimplify[
        SolveValues[{geodesicDistance[R, theta1, phi1, x, y] == 1,
          geodesicDistance[R, theta2, phi2, x, y] == 1}, {x, y}],
        Assumptions -> {1/Pi < R}] /. {C[1] -> 0 , C[2] -> 0} ;
    {theta3, phi3} = sol3[[-1]]
    N[%] /. R -> 1
    (* doesnt converge:*)
    (*sol4 = \
    FullSimplify[SolveValues[{geodesicDistance[R,theta2,phi2,x,y]==1,\
    geodesicDistance[R,theta3,phi3,x,y]==1},{x,y}],Assumptions->{1/Pi<R
    }] \
    /. {Subscript[\[ConstantC], 1]->0 ,Subscript[\[ConstantC], 2] -> 0}
    (*{theta4,phi4} = sol4[[-1]]*)*)



Out[78]= \[Pi] - ArcSin[Cos[1/R]]

Out[79]= 2.5708

    During evaluation of In[73]:= SolveValues::ifun: Inverse functions
    are being used by SolveValues, so some solutions may not be found;
    use Reduce for complete solution information.

Out[81]= {ArcSec[-2 (1 + Cos[1/R]) Csc[2/R]],
     ArcSec[Sqrt[3 + (-2 + Cos[1/R]) Cos[1/R] - 2/(1 + Cos[1/R])] Sec[1/
    R]]}

Out[82]= {1.87043, 0.969759}

In[69]:=
    phi[theta_] :=
      ArcCos[Cot[theta]*C1] +
       C2; (* general expression for geodesic connection between two
    point\
    s *)

    (* e.g. determining C1,C2 for geodesic between (theta2,\
    phi2) and (theta3,phi3): *)
    G1 = phi[theta2] == phi2;
    G2 = phi[theta3] == phi3;

    Solve[G1 && G2, {C1, C2}]

    (* not solvable *)


Out[72]= $Aborted
```

```
    During evaluation of In[1334]:= SolveValues::ifun: Inverse functions
    are being used by SolveValues, so some solutions may not be found;
   use Reduce for complete solution information.
```

Listing B.2: Mathematica code for unsuccesful triangulation.

```
geodesicDistance[R_, \[Theta]1_, \[Phi]1_, \[Theta]2_, \[Phi]2_] :=
R *ArcCos[
    Sin[\[Theta]1] Sin[\[Theta]2] Cos[\[Phi]1 - \[Phi]2] +
    Cos[\[Theta]1] Cos[\[Theta]2]]
Clear[R]
(*R = 1*)
{theta1, phi1} = {2 Pi/5, 0};
phi2 = 0;
sol2 = Simplify[
    SolveValues[geodesicDistance[R, theta1, phi1, x, phi2] == 1, x],
    Assumptions -> 1/Pi < R] /. C[1] -> 0 ;
theta2 = sol2[[1]];

sol3 = N[
    FullSimplify[
    SolveValues[{geodesicDistance[R, theta1, phi1, x, y] == 1,
        geodesicDistance[R, theta2, phi2, x, y] == 1}, {x, y}],
    Assumptions -> {1/Pi < R}]] /. {C[1] -> 0 , C[2] -> 0, R -> 1} ;
{theta3, phi3} = sol3[[4]]
```

Listing B.3: Python code of numerical calculation for finding a geodesic triangulation of the two-sphere.

```
import numpy as np
import matplotlib.pyplot as plt
from scipy.optimize import least_squares
import random

plt.rcParams.update({
    "text.usetex": True,
    "font.family": "serif",
    "font.size": 12,
    "text.latex.preamble": r"""
    \usepackage[T1]{fontenc}
    \usepackage{tgtermes}
    \usepackage[lite,subscriptcorrection,zswash]{mtpro2}
    """,
    # "figure.figsize": (6.2, 4.6), # (6.4, 4.8) standard
})
##########

N = 5 # number of vertices
R = 1 # radius of sphere
s = 1 # edge length (geodetic)

# initialize arrays:
theta = np.zeros(N)
phi = np.zeros(N)

# set start values (first two points):
theta[0] = np.pi/4
phi[0] = np.pi
theta[1] = np.pi/4+1/R
phi[1] = np.pi

```

```
# calculates geodetic distance between two points:
def GeoDist(theta_1,phi_1,theta_2,phi_2):
    return R*np.arccos(np.sin(theta_1)*np.sin(theta_2)*np.cos(phi_1-phi_2)+np.cos(theta_1)*np.cos(theta_2))

# creates system of equations to find roots
def EquSys(theta_1,phi_1,theta_2,phi_2):
    def Func(x):
        return [GeoDist(theta_1,phi_1,x[0],x[1]) - s,
                GeoDist(theta_2,phi_2,x[0],x[1]) - s]
    return Func

# iteratively generate new points:
for k in range(2,N):
    # print("k = ",k)
    test = 1
    while test != 0:
        guesstheta = random.random()*np.pi
        guessphi = random.random()*2*np.pi
        if k % 2 == 1 or k == 2:
            [theta[k],phi[k]] = least_squares(EquSys(theta[k-2],phi[k-2],theta[k-1],phi[k-1]), [guesstheta,guessphi], bounds = ([0, 0], [np.pi, 2*np.pi])).x
        else:
            [theta[k],phi[k]] = least_squares(EquSys(theta[k-4],phi[k-4],theta[k-2],phi[k-2]), [guesstheta,guessphi], bounds = ([0, 0], [np.pi, 2*np.pi])).x

        test = sum(np.logical_and(np.isclose(theta[:k],theta[k]), np.isclose(phi[:k],phi[k]))) # testing variable to eliminate identical points
        # print(theta)
        # print(phi)
        # print(test)


# generate system of equations for determining the coefficients of phi(theta)
def FindConst(theta_1,phi_1,theta_2,phi_2):
    def Func2(x):
        return [np.cos(phi_1-x[1])-x[0]/np.tan(theta_1),
                np.cos(phi_2-x[1])-x[0]/np.tan(theta_2)]
    return Func2

edges = [0,1,0,2,1,2,1,3,2,3,0,4,4,2] # pairs of vertices which contribute to a geodetic edge (0,1),(0,2),...
n = 7
# initializing variables used for plots later:
lam = np.zeros([2*n,100])
phi_par = np.zeros([2*n,100])

# iteritevly calculating geodesics between pairs of vertices defined in edges
for k in range(n):

    C = least_squares(FindConst(theta[edges[2*k]],phi[edges[2*k]],theta[edges[2*k+1]],phi[edges[2*k+1]]), [-2,1]).x
    # print(C)
    # if k == 3:
    #     print(C)
```

```
    lam[k,] = np.linspace(theta[edges[2*k]],theta[edges[2*k+1]],100)
    phi_par[k,] = np.arccos(C[0]/np.tan(lam[k,]))+C[1]


plt.close('all')
# plotting vertices and geodesics between them:
plt.figure()
for k in range(n):
    plt.plot(lam[k,],phi_par[k,],'orange')
plt.plot(theta,phi,"x")
# plt.plot(lam[3,],phi_par[3,]) # 3 seems to be a problem
plt.grid()
plt.xlim([0,np.pi])
plt.ylim([0,2*np.pi])
plt.xlabel(r"$\theta$")
plt.ylabel(r"$\phi$",rotation=np.pi/2)
for i in range(N):
    plt.text(theta[i], phi[i]+0.1,i)
plt.gca().set_aspect('equal')
plt.xticks([0,np.pi/2,np.pi],["0",r"$\pi/2$",r"$\pi$"])
plt.yticks([0,np.pi/2,np.pi,3*np.pi/2,2*np.pi],["0",r"$\pi/2$",r"$\pi$",
   r"$3\pi/2$",r"$2\pi$"])

# 3D-Plot
%matplotlib inline
# %matplotlib qt
fig = plt.figure()
ax = plt.axes(projection='3d')
# plot sphere:
u = np.linspace(0, 2 * np.pi, 100)
v = np.linspace(0, np.pi, 100)
x = R * np.outer(np.cos(u), np.sin(v))
y = R * np.outer(np.sin(u), np.sin(v))
z = R * np.outer(np.ones(np.size(u)), np.cos(v))
ax.plot_wireframe(x, y, z,alpha=0.2,rstride=3, cstride=3)

for k in range(n):
    # plt.figure()
    xline = R*np.sin(lam[k,])*np.cos(phi_par[k,])
    yline = R*np.sin(lam[k,])*np.sin(phi_par[k,])
    zline = R*np.cos(lam[k,])
    ax.plot3D(xline, yline, zline, 'orange',zorder=1)

for i in range(N):
    ax.text(R*np.sin(theta[i])*np.cos(phi[i]),0.1+R*np.sin(theta[i])*np.
   sin(phi[i]),0.05+R*np.cos(theta[i]),i,zorder=2)

ax.set_xlabel(r'$x$')
ax.set_ylabel(r'$y$')
ax.set_zlabel(r'$z$')
ax.set_proj_type('ortho')
ax.set_aspect('equal')
ax.view_init(elev=10, azim=150, roll=0)
ax.set_axis_off()
```

Listing B.4: Mathematica code of test integral for the 2-sphere.

```
In[100]:=
R = 1;
r1[{theta1_, phi1_}] :=
  R*{Sin[theta1]*Cos[phi1], Sin[theta1]*Sin[phi1], Cos[theta1]};
```

```
r2[{theta2_ , phi2_}] :=
  R*{Cos[theta2], Sin[theta2]*Cos[phi2], Sin[theta2]*Sin[phi2]};

r1inv[{x_, y_, z_}] := {ArcCos[z/R], ArcTan[x, y]};
r2inv[{x_, y_, z_}] := {ArcCos[x/R], ArcTan[y, z]};

r12[{theta2_, phi2_}] := r1inv[r2[{theta2, phi2}]];
r21[{theta1_, phi1_}] := r2inv[r1[{theta1, phi1}]];

C1 = -Sqrt[3];
C2 = 3 Pi/2;
x[lambda_] := {lambda, ArcCos[Cot[lambda]/C1] + C2};

FullSimplify[r21[x[\[Lambda]]]]
FullSimplify[D[r21[x[\[Lambda]]], \[Lambda]]]

Out[110]= {ArcCos[Sqrt[1 - Cot[\[Lambda]]^2/3] Sin[\[Lambda]]],
 ArcTan[Cos[\[Lambda]]/Sqrt[3], Cos[\[Lambda]]]}

Out[111]= {-((2 Sqrt[Cos[\[Lambda]]^2] Sec[\[Lambda]])/Sqrt[
  3 - Cot[\[Lambda]]^2]), 0}
```

Declaration

I declare that I have authored this thesis independently, that I have not used other than the declared sources/resources, and that I have explicitly indicated all material which has been quoted either literally or by content from the sources used. The text document uploaded to UNIGRAZonline or TUGRAZonline is identical to the present bachelor's thesis.

Graz, 12th July 2025

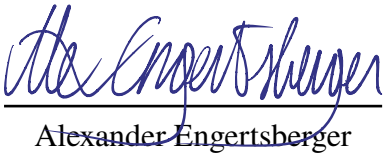

Alexander Engertsberger